RESEARCH ARTICLE

An experimental implication of long-term hot-wet-aged carbon fiber/polyether ketone ketone composites: The impact of automated fiber placement process parameters and process-induced defects

Emine Feyza Sukur[1,2,3] 🔘 | **Sinem Elmas**[2,3,4] | **Volkan Eskizeybek**[5] 🔘 |
Hatice S. Sas[2,3,4] 🔘 | **Mehmet Yildiz**[2,3,4] 🔘

[1]Department of Mechanical Engineering, Faculty of Engineering, Samsun University, Ondokuzmayıs, Samsun, Turkey

[2]Integrated Manufacturing Technologies Research and Application Center, Sabanci University, Pendik, Istanbul, Turkey

[3]Composite Technologies Center of Excellence, Sabanci University-Kordsa, Istanbul Technology Development Zone, Pendik, Istanbul, Turkey

[4]Faculty of Engineering and Natural Sciences, Sabanci University, Istanbul, Turkey

[5]Department of Materials Science and Engineering, Faculty of Engineering, Canakkale Onsekiz Mart University, Canakkale, Turkey

Correspondence
Mehmet Yildiz, Integrated Manufacturing Technologies Research and Application Center, Sabanci University, Pendik, Istanbul 34906, Turkey.
Email: mehmet.yildiz@sabanciuniv.edu

Abstract

During the service life of aerospace-grade composites, process parameters and process-induced defects may become crucial. Most studies in this field have mainly focused on the relationship between process-induced defects and mechanical performance. However, the potential impact of process parameters and process-induced defects on the service life of composites serving under severe service conditions has received little attention. In this work, the effects of hydrothermal conditioning on the mechanical performance of carbon fiber/polyether ketone ketone (CF/PEKK) composites are examined, along with the correlation between automated fiber placement (AFP) process parameters and process-induced defects. For this, gap and overlap defects integrated CF/PEKK laminates were exposed to a long-term (90 days) hot-wet aging environment to simulate the actual service conditions. Defect-induced composite samples reached saturation point at the end of 30 days with a mass gain of 0.2 wt%. The aging process resulted in an increase in the degree of crystallization by almost 14% without a change in the chemical structure, indicating the post-crystallization of the PEKK matrix. Even though the thermo-mechanical performance diminished (∼25%) with the aging process, storage modulus was slightly affected by process parameters and process-induced defects. Considering the flexural and shear test results after the aging process, the impact of gap and overlap defects on the service life of AFP composites can be minimized with higher compaction forces (600 N) and lower lay-up speeds (0.1 m/s).

KEYWORDS
automated fiber placement (AFP), hydrothermal aging, process-induced defects, thermoplastic composites

1 | INTRODUCTION

The aerospace industry is highly demanding of thermoplastic polymer composites because of their potential to reduce the weight of aircraft structures by 20%–50% compared with thermoset and metallic solutions, respectively. Therefore, there has been tremendous growth in the use of high-performance thermoplastic polymer composites in the aerospace industry due to their lightweight, high fracture toughness, damage tolerance, recyclability, and long service life.[1–3] The mechanical performance of polyetheretherketone (PEEK) and polyether ketone ketone (PEKK), two significant members of the high-performance thermoplastic family, has received the most attention in order to meet the increasing needs of next-generation aerospace constructions.[4] Nonetheless, a relatively small number of research have been done on the aging behavior of high-performance thermoplastic composites. In general, the aging of aerospace-grade composites is affected by a variety of parameters, (i) moisture content and exposure time, (ii) temperature and environmental conditions (UV radiation, and harsh chemicals), (iii) material properties, and (iv) the manufacturing process (process parameters, process-induced defects).[5]

With the increasing use of thermoplastic composites in primary structural parts of an aircraft, advanced manufacturing techniques have become necessary for producing large and complex geometry parts in a shorter period with low-cost, high accuracy, and production quality.[6,7] Advanced manufacturing technologies mainly include automated and robotic processes like automated tape laying and automated fiber placement (AFP). In the AFP process, a robotic placement head lays up preimpregnated fibers in different orientations over preheated flat or curved surfaces with specific process parameters, including nip point temperature, tool temperature, compaction force, lay-up speed, laser spot size, and angle.[8,9] The selection of process parameters is critical in producing defect-free composite parts. Among these process parameters, temperature, lay-up speed, and compaction force are the crucial parameters affecting the material properties and mechanical performance of AFP layered composite structures, such as crystallinity, through-thickness void fraction, degree of bonding, interlaminar shear strength (ILSS), and fracture toughness.[10,11] In addition to void formation and other defects, process-induced defects occur specifically in the AFP process, such as gap, overlap, pucker, wrinkle, bridging, boundary coverage, angle deviation, fold, twist, splice, position error, and others.[12]

The effect of various defects on AFP-manufactured polymer composite laminates quality and consequently on the mechanical performance has been investigated for different defect types and distribution, material systems, and loading conditions with several numerical and experimental studies by many scholars.[13–18] The researchers have focused on gaps and overlaps, the most common defects during AFP placement, resulting in either a decrease or increase in the local thickness of the laminate.[18]

Composite structures, especially aircraft parts, are designed to perform in extreme service conditions. For example, during the taxiing, the heat generated by engines is reflected by the ground to the main body and wings of the aircraft, which is absorbed by the structural members depending on the taxiing duration. Since the taxiing duration can be long enough depending on the traffic, the reflected heat can lead to hydrothermal aging, specifically in warm weather conditions. In addition, manufacturing-induced defects can become critical under service conditions. The types, distribution, and amount of defects alone are insufficient to predict the possible reduction of mechanical performance,[18] and their effects on service conditions need to be examined. Hydrothermal aging by hot-water absorption induces different physical or chemical effects on the composites, such as (i) plasticization or antiplasticization of the matrix, (ii) swelling and induced internal stresses, cracking/crazing due to osmosis, and (iii) damage of the fiber/matrix interface due to water presence.[19–21] Borba et al.[22] applied hydrothermal aging on the CF-PEEK composite and CF-PEEK friction riveted joints at 71°C and 95% relative humidity for 28 days. After the aging process, riveted joints showed an increase in the degree of crystallinity (7%) with various physicochemical changes, including the formation of phenol groups, aliphatic polyether groups, and degraded aromatic polyether groups. Plagianakos et al.[23] performed various mechanical tests on CF/PEEK woven composites conditioned at 80°C and 85% relative humidity. They revealed that matrix-dominated mechanical properties exhibited predominant degradation after aging. Mazur et al.[24] presented the influence of accelerated aging on the compression and shear properties of carbon fiber/polyether ketone ketone (CF/PEKK) composites conditioned at 80°C and 90% relative humidity for 6 weeks. They reported a significant enhancement in the compression and shear properties of the composites as an indication of the antiplasticization effect. Nevertheless, the existing literature does not attempt to consider the potential impact of process-induced defects on hydrothermally conditioned aerospace-graded fiber-reinforced composites.

In this work, the relationship between process parameters, process-induced defects, and the effects of hydrothermal aging on the mechanical performance of CF/PEKK composites have been extensively investigated.

First, gap and overlap defect-embedded CF/PEKK laminates were produced using AFP by three sets of process parameters varied with compaction force and lay-up speed. The effect of the process parameters on the composite quality was evaluated by void ratio analysis. In the second phase, the laminates were exposed to a long-term hot-wet aging environment to simulate the actual service conditions of aerospace composites. We systematically performed structural and mechanical tests on the conditioned composite samples. According to obtained results, the present study fills a gap in the literature considering the impact of manufacturing-induced defects and long-term hydrothermal aging on the durability of fiber-reinforced thermoplastic composites.

2 | EXPERIMENTAL METHODS

2.1 | Materials

Unidirectional (UD) carbon fiber reinforced PEKK thermoplastic tape (TORAY Cetex®TC1320 PEKK. AS4D UD Tape 145 g/m². 1/4″ wide slitted tape) was purchased from Toray Advanced Composites (USA). For the tapes, the resin content was 34 wt%, and the density was 1.59 g/cm³, according to the supplier datasheet (Table 1).

2.2 | Manufacturing of composite laminates with AFP

Temperature, compaction force, and lay-up speed allow a successful bonding by removing the first roughness in the strip during the thermoplastic AFP manufacturing process. This study examines the effects of two different compaction forces and two different lay-up speeds on defect formation and mechanical performance. The limits of low and high compaction force in our study were determined as 300 and 600 N, respectively, by considering material preferences and current literature

studies.[4,25–28] Lay-up speed is the most significant indicator of the efficiency in the AFP process, and it should be high as possible to increase production rates. However, the demands of quality, repeatability, and accuracy of laying restrict high-level lay-up speeds.[29] Based on the lay-up speed values studied in the literature, the lay-up speed limits are determined as 0.1 and 0.4 m/s for low and high lay-up speeds, respectively.[30]

CF/PEKK composite laminates were manufactured by Coriolis C1 (Coriolis Composites) laser-assisted AFP system with a KUKA QUANTEC KR210R3100 robot with different process parameters given in Table 2 with the dimensions of $40 \times 60 \times 3 \pm 0.1$ mm³ by laying up 20-layer CF/PEKK tapes onto a heated stainless steel tool at 130°C. The tool surface was covered with a 50 μm thick polyimide film (Thermalimide RCBS, Airtech Advanced Materials, UK) to ensure the easy separation of laminate. To control the temperature during laying, seven thermocouples connected to the control unit were placed in the tool corners. Each tape consists of 8 tows, and all 8 tows in the tape were selected for manufacturing defect-free composite laminates. Three defect-free reference laminates were produced for each process parameter set (Set 1, Set 2, and Set 3) as given in Table 2, and named as Reference. AFP lay-up and autoclave process are represented in Figure 1.

In addition to reference composite laminates, gap and overlap defect-induced composite laminates (Figure 2) were manufactured with the same process parameters (Table 2). In order to better understand the effects of the service conditions (moisture/water absorption) on the mechanical performance of the defect-embedded composites, the defects were created in the unsymmetrical layers close to the final layer. The second and seventh tows in the tape were not laid up in the 14th and 15th layers of the laminate during the AFP process to introduce the gap defect. To generate overlap defects, two additional layers, 14.1 and 14.2, were assigned at the 14th and 15th layers of the laminate, and overlap defects were created by selecting the second and seventh tows in each strip of both layers (Figure 2).

TABLE 1 Physical properties of Carbon/ PEKK UD tape.

Property	Standard modulus carbon UD tape
Fiber areal weight	145 g/m²
Weight per ply	221 g/m²
Resin content by weight	34%
Consolidated ply thickness	0.14 mm
Density	1.59 g/cm³
Width	305 mm

TABLE 2 AFP process parameters.

| CF/PEKK laminates | Process parameters | |
	Compaction force (N)	Lay-up speed (m/s)
Set 1_Reference	300	0.1
Set 2_Reference	600	0.1
Set 3_Reference	600	0.4
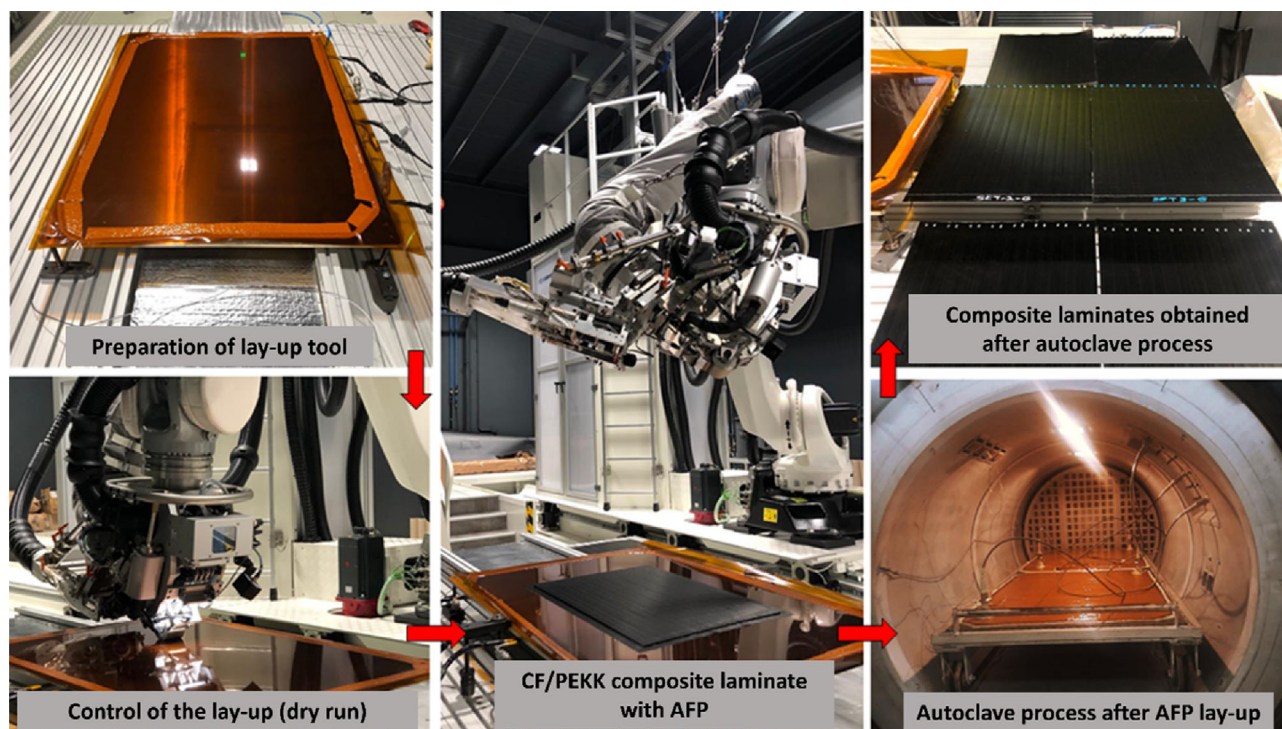
FIGURE 1 CF/PEKK laminates lay-up and autoclave process. [Color figure can be viewed at wileyonlinelibrary.com]
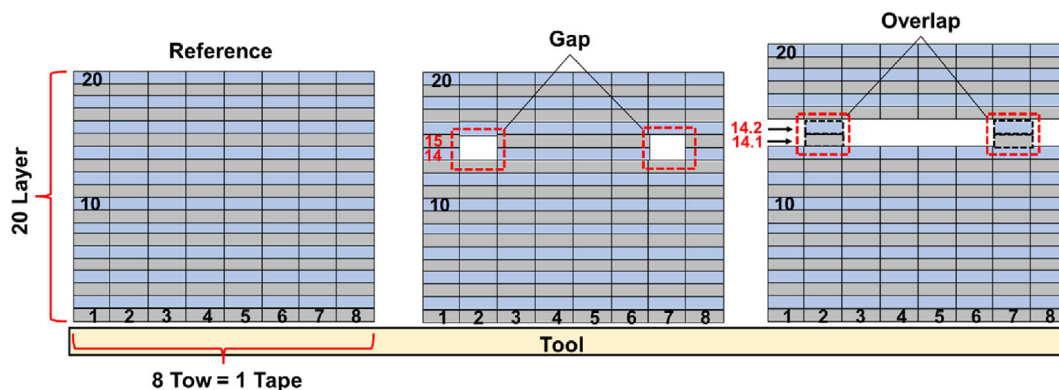

FIGURE 2 Schematic representation of reference, gap, and overlap defect embedded laminates. [Color figure can be viewed at wileyonlinelibrary.com]

The autoclave consolidation was realized to CF/PEKK laminates after the lay-up process to produce high-quality laminates for the aerospace industry. For this, the laminates were heated to 377°C from room temperature with a 5°C/min heating rate. When the autoclave temperature reached at 377°C, the pressure was increased to 0.8 MPa in 25 min and the laminates were consolidated at 0.8 MPa and 377°C for 40 min. Later, laminates were cooled to room temperature with an 11°C/min cooling rate. Then, the autoclave-consolidated laminates were cut with a water jet (KUKA—KR 16–2 C-F) in accordance with the standards specified for mechanical testing and characterization.

2.3 | Characterization and mechanical tests

2.3.1 | Void analysis

CF/PEKK composite laminate density was measured according to ASTM D792 standard through water buoyancy. The matrix digestion method was conducted twice for each sample to analyze the fiber volume fraction and the void content with the acid treatment procedure described in ASTM D3171/Method B. The void content was calculated by using Equation (1).

$$V_v = 100 - \left(V_f + V_m\right)$$

$$V_f = \rho_c \frac{W_f}{\rho_f} \text{ and } V_m = \rho_m \frac{W_m}{\rho_m}, \qquad (1)$$

where V_v, V_f, and V_m are the volume content (%) of the void, fiber, and matrix; ρ_c, ρ_f, and ρ_m are the density (g/cm^3) of the composite fiber and the matrix; W_f and W_m are the weight percentage of the fiber and the matrix, respectively.

The void content and distribution into composite laminates were also supported by optic microscopy (Nikon—LV100ND) images. The samples were molded into silicon mold using epoxy, and then surface polishing was applied. The microscopy images were taken at 50× and 100× magnifications and converted to black and white images. The volume fraction of voids was calculated from the microscopy images using image processing methods as described by Gangloff et al.[31]

2.3.2 | Hydrothermal aging of CF/PEKK laminates

Hydrothermal aging conditioning was designed according to ASTM D5229M-12. Samples were dried in an oven at 70°C to eliminate moisture content, and the samples were weighed before the hydrothermal aging. After, CF/PEKK composite samples were put into a hot water bath at 70°C for accelerated hydrothermal aging. The samples were weighed periodically during the 3 months of the hydrothermal aging period, and the water uptake content M (average moisture content) was calculated using Equation (2). The mass gain results given for CF/PEKK composites are the average values of three samples.

$$M(\%) = \frac{W_i - W_0}{W_0} \times 100, \qquad (2)$$

where W_0 and W_i are initial mass and water absorbed mass, respectively.

2.3.3 | Material characterization

To analyze the glass transition temperature (T_g), melting (T_m), and crystallization (T_c) temperatures and enthalpies of CF/PEKK composites, differential scanning calorimetry (DSC) measurements were carried out by Mettler Toledo 821 DSC 3+ instrument under the nitrogen atmosphere in the temperature range of 25–400°C with a 5°C/min heating and cooling rate and the test is repeated

two times. The degree of crystallinity (X_c) was calculated by using Equation (3);

$$X_c = \frac{\Delta H_m}{\Delta H_m^\circ \times W_m} \times 100, \qquad (3)$$

where X_c is the degree of crystallinity, W_m is the matrix weight fraction. ΔH_m, and ΔH_m° are the melting enthalpy obtained from the melting peak and melting enthalpy account for PEKK material with 100% crystallinity (130 J/g),[32] respectively.

Thermogravimetric analysis (TGA) was carried out by Mettler Toledo TGA- DSC 3+ in the temperature range of 25–1000°C with a 10°C/min heating rate under the nitrogen atmosphere to analyze the degradation with two repeats. Structural analysis was utilized using Fourier transform infrared (FTIR) spectroscopy (Thermo Scientific Nicolet™ iS50) to correlate the impact of hydrothermal aging and mechanical properties in a transmission mode. The spectra were recorded as the average of 16 scans in the range of 4000–650 cm^{-1} with a spectral resolution of 4 cm^{-1}. Dynamic mechanical analysis (DMA) and short beam shear (SBS) tests were carried out to analyze the effect of process parameters and service conditions on mechanical performance. DMA analysis was performed by Mettler Toledo DMA/SDTA861e instrument in dual cantilever mode according to ASTM D4065 standard over a temperature range of 25–250°C with a 3°C/min heating rate at 1.00 Hz frequency with two repeats. SBS test was performed according to ASTM D2344 standard and was conducted five times on an Instron Universal Testing Machine (5982) equipped with a static load cell of ±100 kN. SBS strength values of composite samples were calculated by using Equation (4);

$$F^{SBS} = 0.75 \times \frac{P_m}{b \times h}, \qquad (4)$$

where P_m is the maximum load, b and h are sample width and thickness, respectively.

3 | RESULTS AND DISCUSSION

3.1 | Optical microscopy images

The images obtained from the optical microscopy are given in Figures 3–5. Similar optical microscopy images are obtained from reference laminates manufactured with Set 1, Set 2, and Set 3 process parameters, as given in Figure 3 with the thickness values of 3.05, 2.91, and 3.04 mm, in the given order. As can be seen in Figure 3, the high lay-up speed results in resin-rich regions
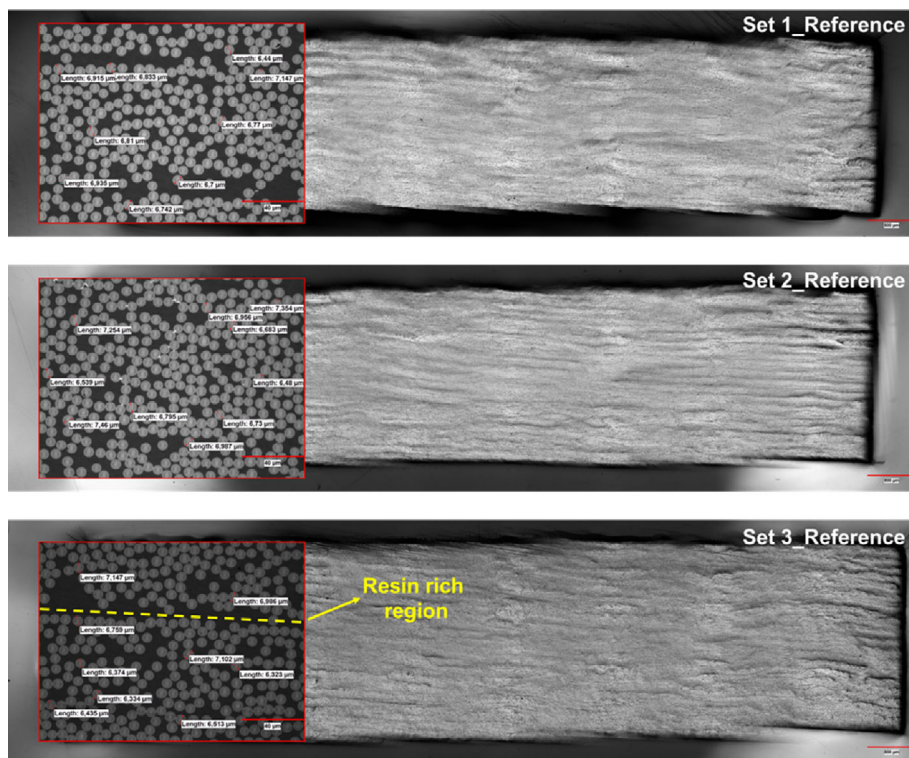
FIGURE 3 Optical microscopy images of reference laminates manufactured by Set 1, Set 2, and Set 3 process parameters. [Color figure can be viewed at wileyonlinelibrary.com]

between the layers with lower final intimate contact (Set3_Reference), compared with low lay-up speeds (Set1_Reference and Set2_Reference).[33,34]

Different consolidation mechanisms are visualized in defect-embedded composite laminates. Compacted geometry and the embedded defects depend on the defect size of the laminate and stacking order.[18] In the case of a gap defect (Figure 4), adjacent layers above the fourteenth layer flow into the gap defect. The layers that border the defect spread inward and form a tapering shape with small matrix pockets that are visible at high magnifications. The fibers cannot interosculate due to the natural geometry and continuity of the fibers. Consequently, the top layer (or strip) leans over the bottom layer. The curvature and the contact point of the top and bottom layers can change depending on the bending stiffness of the top layer.

For the overlap defect (Figure 5), two strips with the same fiber orientation are stacked on top. The gap regions on the top surface create a concave form, while the overlapping regions on the top create a convex form. The fibers in both strips move with low resistance, and the stripes appear to coalesce when the matrix becomes liquid during the autoclave process. The ply-merging phenomenon develops while resin-rich regions are formed when the defects overlap.[14] The effects of the gap and overlap defects, which showed different consolidation mechanisms in optical microscopy images, on the thermo-mechanical

properties and aging behavior of CF/PEKK composites are discussed in detail.

3.2 | Density measurement and void content analyses results

Composite laminate production following aerospace industry standards was aimed within the scope of the study. Density, fiber volume fraction and void fractions of reference, and gap and overlap defect-embedded CF/PEKK composite laminates manufactured with different process parameters are given in Table 3. The acceptable critical void content of advanced composites is below 1 vol% for aerospace applications. Although it is broadly known that more than 1 vol% void content in composites adversely affects the mechanical properties, the void content can vary between 1 and 2 vol% or even 5 vol% depending on different application areas.[34,35]

Two types of voids form as intralaminar and interlaminar with the in situ consolidation in the AFP process. The intralaminar voids form during the strip impregnation stage, while the interlaminar void is primarily the result of strip insertion. The intralaminar void is embedded in the strip. Gruber et al.[36] suggested that automatic tow lay-up could not reduce the intralaminar void content. The void fraction of AFP-manufactured composite laminates is reduced by secondary consolidation

FIGURE 4 Optical microscopy images of gap defects included laminates manufactured by Set 1, Set 2, and Set 3 process parameters. [Color figure can be viewed at wileyonlinelibrary.com]
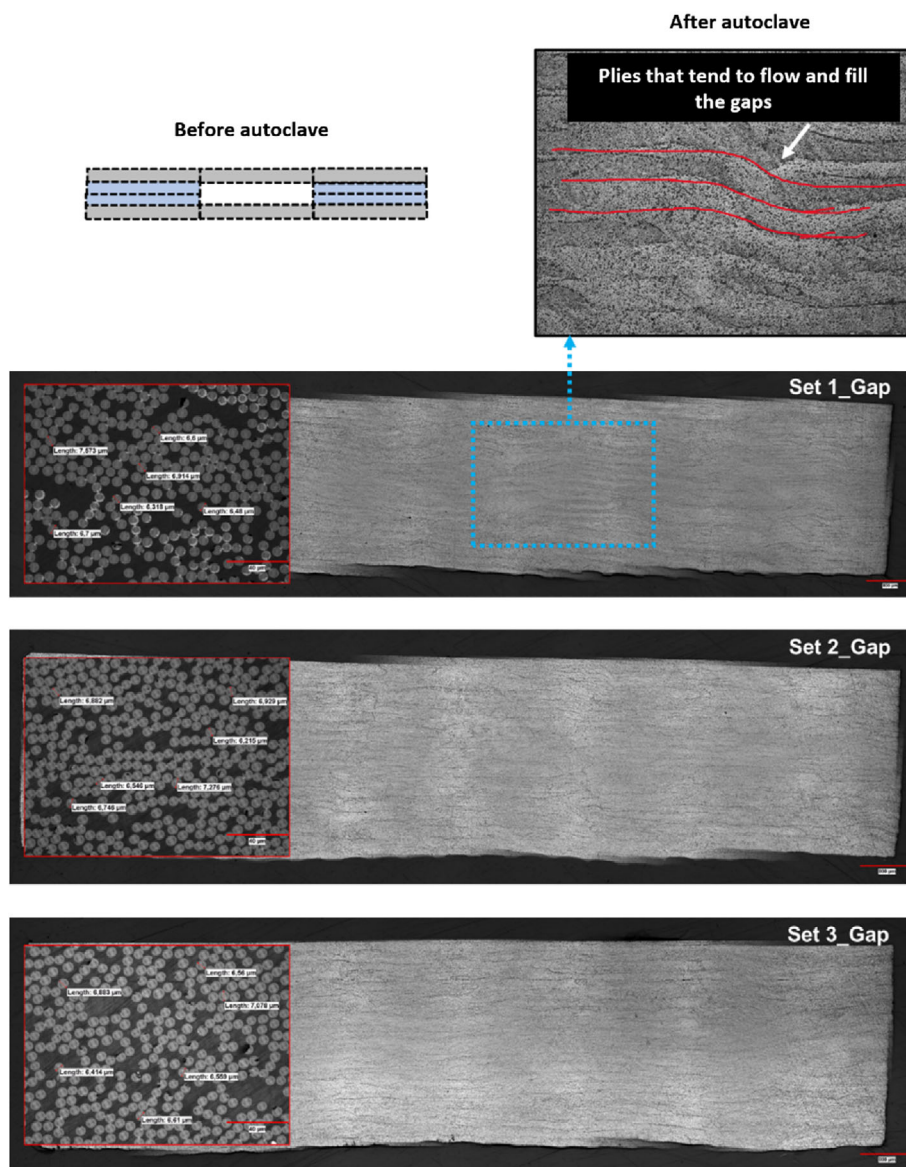
processes to meet the low void content of aerospace industry requirements.

In the literature, various secondary processes such as annealing, autoclave, hot press, and vacuum bagging have been applied to minimize the void content and improve the mechanical properties of thermoplastic composites after AFP lay-up. In previous studies, the secondary processes are eliminated, and the composite part is manufactured with in situ consolidation in the AFP process. In this context, a preliminary lay-up was carried out at 300 N and 0.1 m/s, this study's lowest consolidation force and lay-up speed parameters. The void ratios of these composite laminates, including gap and overlap defects, vary between 0.14–0.33 vol%, as confirmed by optical microscopy analyses. The void contents of all samples are below 1 vol%, which is a necessity for the aerospace industry. The attention-getter point is the lower

void content at a low consolidation force. It is expected that the void content will minimize as the consolidation force increases, but the void ratio of the Set 2_Reference sample manufactured with 600 N consolidation force is higher than the Set 1_Reference sample manufactured with 300 N consolidation force. This result can be elucidated by obtaining a lower void ratio by creating an air evacuation channel between the layers in the vacuum bagging processes of the prepregs, making it possible to evacuate the air inside the prepregs quickly. In the laminates manufactured with low consolidation force (Set 1_Reference), the interlaminar air evacuation channels are wider to facilitate the release of the existing voids compared with the composite laminate manufactured with high consolidation force (Set 2_Reference) before the autoclave process, improving the quality of the composite.
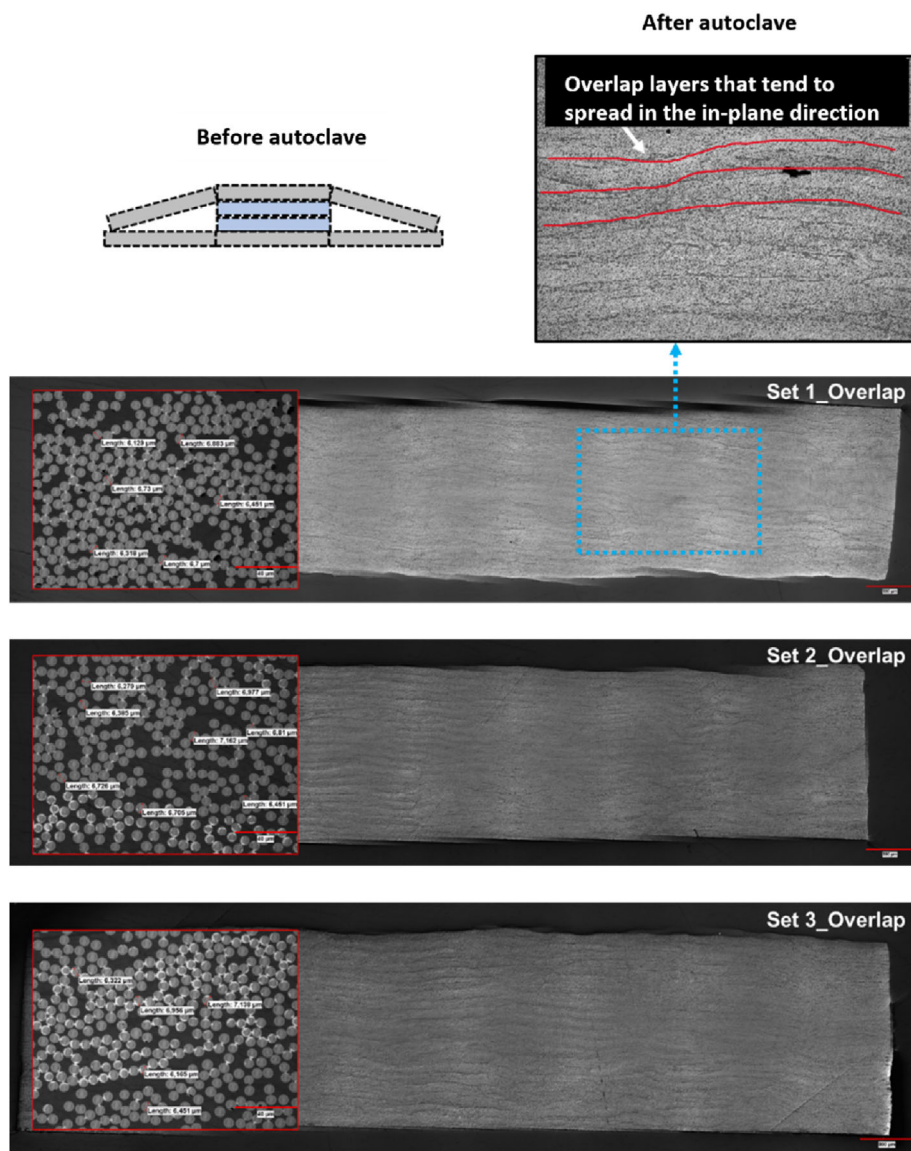
FIGURE 5 Optical microscopy images of overlap defects included laminates manufactured by Set 1, Set 2, and Set 3 process parameters. [Color figure can be viewed at wileyonlinelibrary.com]

3.3 | Accelerated hydrothermal aging results

Figure 6 shows the mass gain as a function of the aging time of Reference samples. Each data point on the mass gain curve is the average value of the three samples. It is clear that the mass gain increases quickly in the early stages of the aging period (up to 20 days) and reaches saturation with a maximum value of 0.20 wt% mass gain after 30 days. There is no significant change in the weight of the samples after reaching saturation point until the end of 90 days. This trend is generally observed in aging processes performed in a water bath with a temperature higher than room temperature for polymer composites. It can be attributed to the rise in water diffusion as a function of temperature.[37,38] The mass gain is almost at the same level (0.20 wt%) for all samples since the void fractions are close.

Mazur et al.[24] reported that CF/PEKK composite samples reached the saturation limit with water absorption of approximately 0.22% after 6 weeks of aging at 80°C and 90% RH. Mass gain results of CF/PEKK samples in the current study are compatible with the literature. Water absorption into polymer composite occurs by diffusion of water molecules from the sample surface toward the center of the section. Furthermore, water can also be absorbed through microcracks, voids, or any discontinuity between the fiber and polymer matrix due to capillarity. The literature states that, for semicrystalline polymers, water can penetrate the amorphous region more quickly than the crystalline region and acts as a plasticizer rather than a solvent.[39] As stated in various studies, the plasticization/antiplasticization/swelling phenomenon reduces the T_g of thermoplastic polymers and causes impairment in mechanical properties such as strength, modulus, and stiffness.[40] The mass gain of

TABLE 3 CF/PEKK composite laminates' density, fiber/matrix weight fraction, and void volume contents after the autoclave process.

		Set 1	Set 2	Set 3
Gap	W_r	64.80	64.79	65.11
	W_m	35.20	35.21	34.89
	V_v	0.27	0.14	0.19
	ρ_c	1.58	1.58	1.58
Overlap	W_r	64.61	64.80	64.92
	W_m	35.39	35.20	35.08
	V_v	0.28	0.33	0.12
	ρ_c	1.57	1.58	1.58
Reference	W_r	63.85	64.58	64.02
	Wm	36.15	35.42	35.98
	V_v	0.20	0.25	0.26
	ρ_c	1.57	1.57	1.57

Note: W_r, fiber weight fraction (%); V_v, void volume content (%); W_m, matrix weight fraction (%); ρ_c, composite density (g/cm^3).
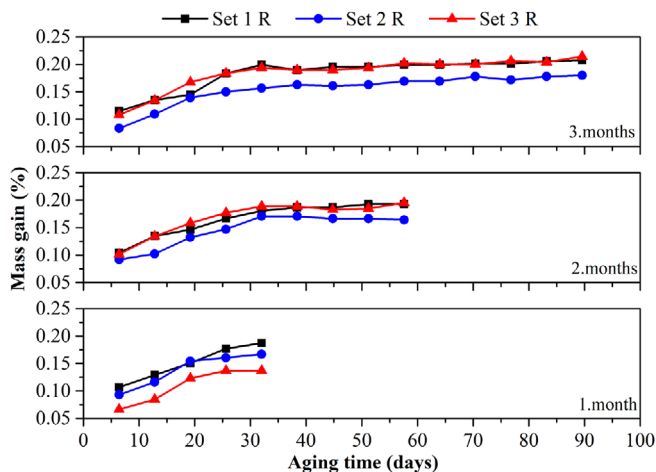
FIGURE 6 Mass gain percentage (%) of the reference CF/PEKK composite samples manufactured with process parameters Set 1, Set 2, and Set 3 as a function of the aging period. [Color figure can be viewed at wileyonlinelibrary.com]

FIGURE 7 Mass gain percentage (%) of reference, gap, and overlap included CF/PEKK samples manufactured under the same process parameters (Set 1). [Color figure can be viewed at wileyonlinelibrary.com]

composite laminates manufactured with Set 1 parameters is given in Figure 7. This graph discusses the effect of gap and overlap defects on the water absorption of CF/PEKK composites. Other effects of process parameters are given in supplementary data. The mass gain increased rapidly during the early stages of the aging period (up to 20 days). It reached saturation with a maximum value of 0.20 wt% after 30 days in the reference and gap defect-embedded composite samples. As discussed before, the mass gain percentages are expected to be close to each other depending on the determined void fractions. For
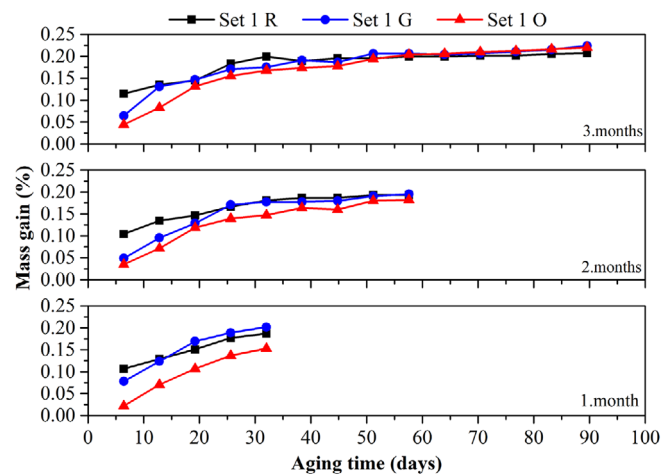
the composite samples that overlap defect-induced composite laminates, the mass gain percentages show a linear increase in the early stages of the aging period. However, it absorbs less water than the other composite laminates, reaching the saturation limit at 0.15 wt%. In the samples, including the overlap defect, two excess tows were laid up in each strip in two layers. It is thought that overlap defects cause a decrease in water absorption into composite samples since the matrix dominates the water absorption.

3.4 | Thermal analysis results

DSC analyzes were utilized to investigate the effect of hydrothermal aging on the glass transition temperature (T_g), melting temperature (T_m), crystallization temperature (T_c), melting/crystallization enthalpies, and crystallization degree of CF/PEKK composites. The heating and cooling curves of the CF/PEKK samples before aging (BA) are given in Figure 8a,b, and the heating and cooling curves of the CF/PEKK samples after aging (AA) are presented in Figure 8c,d, respectively. Initial heating curves are used to evaluate the thermal history of the material and provide information about the effect of hydrothermal aging on the thermomechanical properties of composites.[22] However, the weight of samples (~5 mg) used in DSC analysis is quite limited. Therefore, the analysis results do not give sufficiently reliable results for T_g. Thus, the effect of aging processes on T_g is discussed in detail and more sensitive in the results of DMA analysis, as suggested in the literature. There are no significant differences in T_g, T_m, and T_c values at the end of 3 months
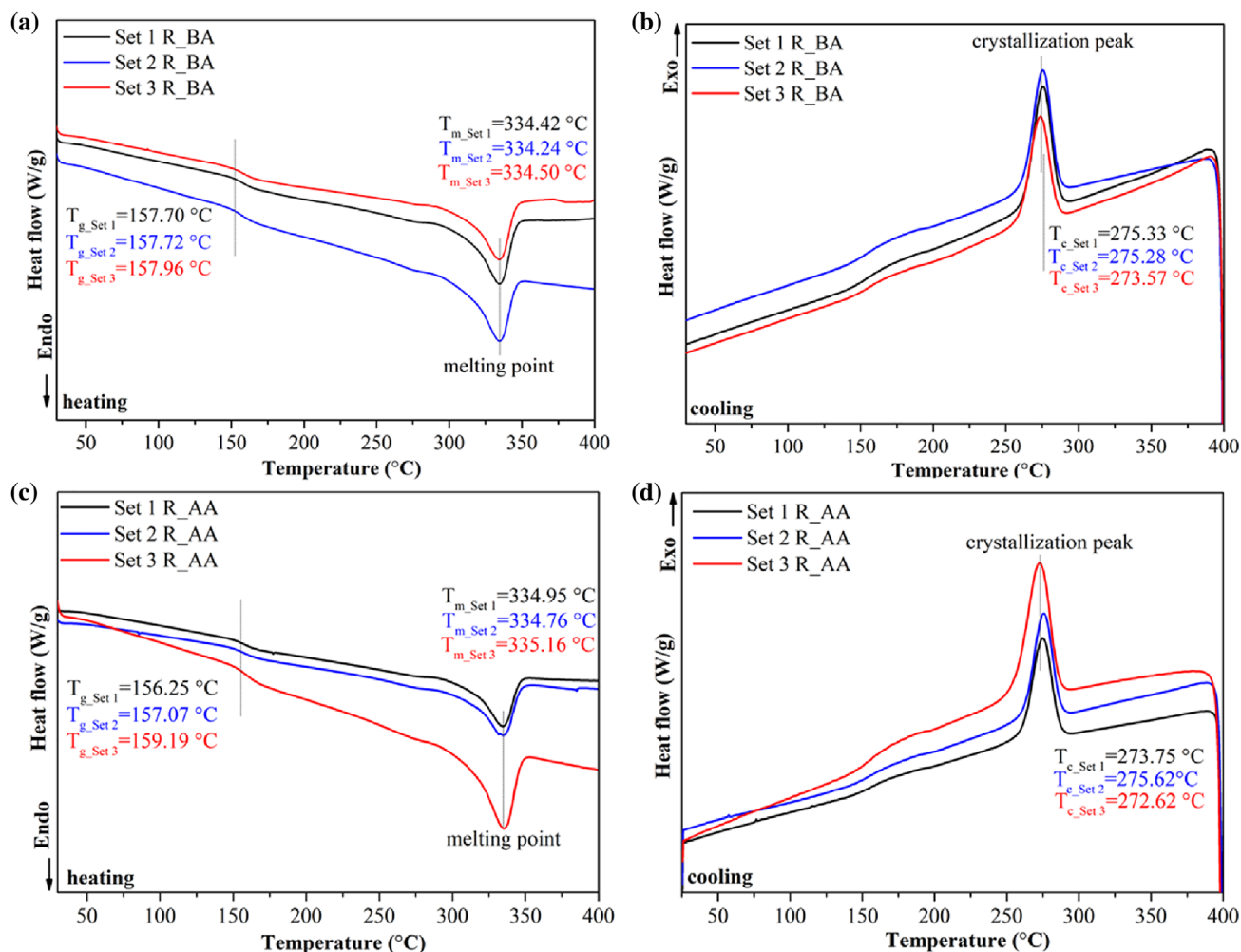
FIGURE 8 DSC curves of CF/PEKK composites: (a) BA heating, (b) BA cooling, (c) AA heating, (d) AA cooling. [Color figure can be viewed at wileyonlinelibrary.com]

aging period, as can be seen from the temperature values corresponding to the peak points of the DSC curves. In the meantime, the intensity of peak (enthalpy values) shifts, indicating the change in crystallization degrees of the CF/PEKK composite samples.

The crystallization degrees are calculated from the melting enthalpy values of the CF/PEKK samples manufactured with the parameters of Set 1, Set 2, and Set 3 before aging are 26.07%, 27.91%, and 25.74%, respectively. The enthalpy values increase after aging; hence, the crystallization degrees increase, which are 29.75%, 30.34%, and 28.39%, respectively. There is an improvement in crystallization degrees 14.11%, 8.70%, and 10.29% manufactured with process parameters Set 1, Set 2, and Set 3, respectively. The improvement can be attributed to the postcrystallization of the matrix with the aid of temperature and water, which allows the polymer chains in the amorphous regions to gain sufficient mobility to break off and recrystallize.[22]

The thermograms of CF/PEKK composites obtained from TGA analyses are given in Figure 9. There is no change in the total mass loss of CF/PEKK composite samples before and after aging. In addition, it is observed that the temperatures of 1% weight loss $T1$ (°C) of composites are lower after the aging; 15.63, 11.56, and 11.34°C in Set 1, Set 2, and Set 3 sample groups, respectively (Table 4). The results indicate a drop in thermal stability due to the decrease in temperatures of % weight in all three sample groups after hydrothermal aging. The decline in thermal stability can be attributed to the synergetic effects of thermal and hydrolytic degradation.[41]

3.5 | Chemical structure analysis by Fourier transform infrared spectroscopy

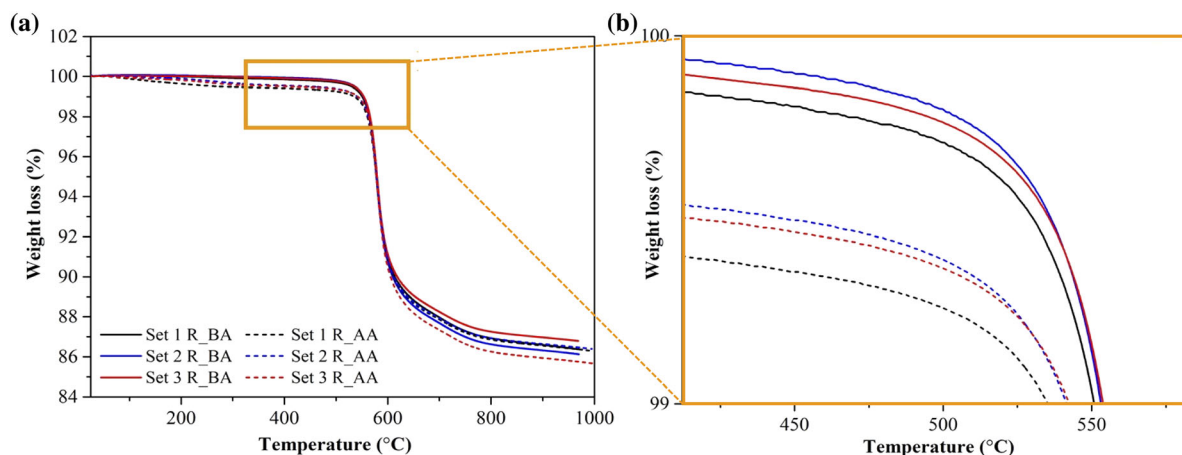The FTIR spectra before and after 3-months of hydrothermal aging of CF/PEKK samples are given in Figure 10.

FIGURE 9 TGA thermograms of CF/PEKK samples manufactured by Set 1, Set 2, and Set 3 process parameters before and after aging. [Color figure can be viewed at wileyonlinelibrary.com]

TABLE 4 TGA data of CF/PEKK composites before and after aging.

CF/PEKK laminates	The temperature of % weight loss		
	$T1$ (°C)	$T5$ (°C)	$T10$ (°C)
Set 1_R_BA	550.74	577.96	613.60
Set 2_R_BA	558.39	589.33	621.67
Set 3_R_BA	559.33	590.33	630.37
Set 1_R_AA	535.11	577.81	610.68
Set 2_R_AA	546.83	581.83	615.33
Set 3_R_AA	547.99	580.83	607.50

Figure 10a–c represents the FTIR spectra of CF/PEKK composite samples manufactured by the parameters Set 1, Set 2, and Set 3, respectively. Two important members of the poly aryl ether ketone family, PEEK, and PEKK, have very similar chemical structures except for the ratio of ketone groups (33% in PEEK and 66% in PEKK).[42] The fingerprint region of the PEKK spectrum is between 1700 and 650 cm^{-1} in the FTIR spectrum.[43] The specific bond groups of the PEKK molecule are the C–H bonds of the benzene ring, the C=O bond of ketone, the C=C bond of the aromatic ring, and the ether bond (CO).[44] These characteristic peaks of PEKK are observed in the CF/PEKK composite samples before and after aging. The peaks at 1644, 1493, and 920 cm^{-1} are attributed to the diphenyl ketone group. The peak at 1584 cm^{-1} is attributed to the C=C stretching vibrations in the aromatic ring.[45,46] C–O bonds of carbonyl asymmetric stretching peaks are observed at 1401 and 1305 cm^{-1}, belonging to ketone bending motion and diphenyl ether group properties.[38,45] The peaks at 1229 and 1153 cm^{-1} belong to the asymmetric stretching vibration peaks of the C–O–C bond in diaryl groups.[46,47] At 1105 and 1012 cm^{-1}, additional peaks of ether groups appear.[43] C–H groups are present in the peaks at 838, 743, and 693 cm^{-1}.[48] C–H bending vibration peaks outside the plane of the benzene ring are observed at 838 and 743 cm^{-1}.[49,50] The peak proves hydroxyl group (–OH) presence at 3307 cm^{-1}.[22]

The appearance of characteristic peaks of the PEKK molecule before and after aging without any new peaks or peak shifts indicates that the hydrothermal aging process causes no chemical change in CF/PEKK composites (Figure 11). On the other hand, there was an increase in the peak intensities of hydroxyl groups (3307 cm^{-1}), diphenyl ketone group (1644, 1493, 920 cm^{-1}), C=C stretching vibration in the aromatic ring (1584 cm^{-1}), and C–O–C asymmetric stretching vibration (1229, 1153 cm^{-1}) in CF/PEKK samples manufactured with three different process parameters that were consistent with the literature studies.[4] These increases in peak intensities are enhanced with the physical aging period. The change in peak intensities can be attributed to an increment in the mass gain with the aging period. Absorbed water can be directly related to the increase in hydroxyl peak intensities. FTIR spectroscopy can be utilized effectively to measure the degree of crystallinity in PEEK polymers, as stated in the literature. The crystallinity degree of CF/PEKK samples BA and AA can be calculated comparatively by the height ratio of corresponding peaks in the FTIR spectrum between the range of 1305 and 1280 cm^{-1}.[46] The slight decrease in the intensity of corresponding peaks is directly related to the increase in the absorbance, hence the increase in crystallinity of the CF/PEKK samples after hydrothermal aging. These findings are complimentary with the results obtained from DSC analyses after aging.
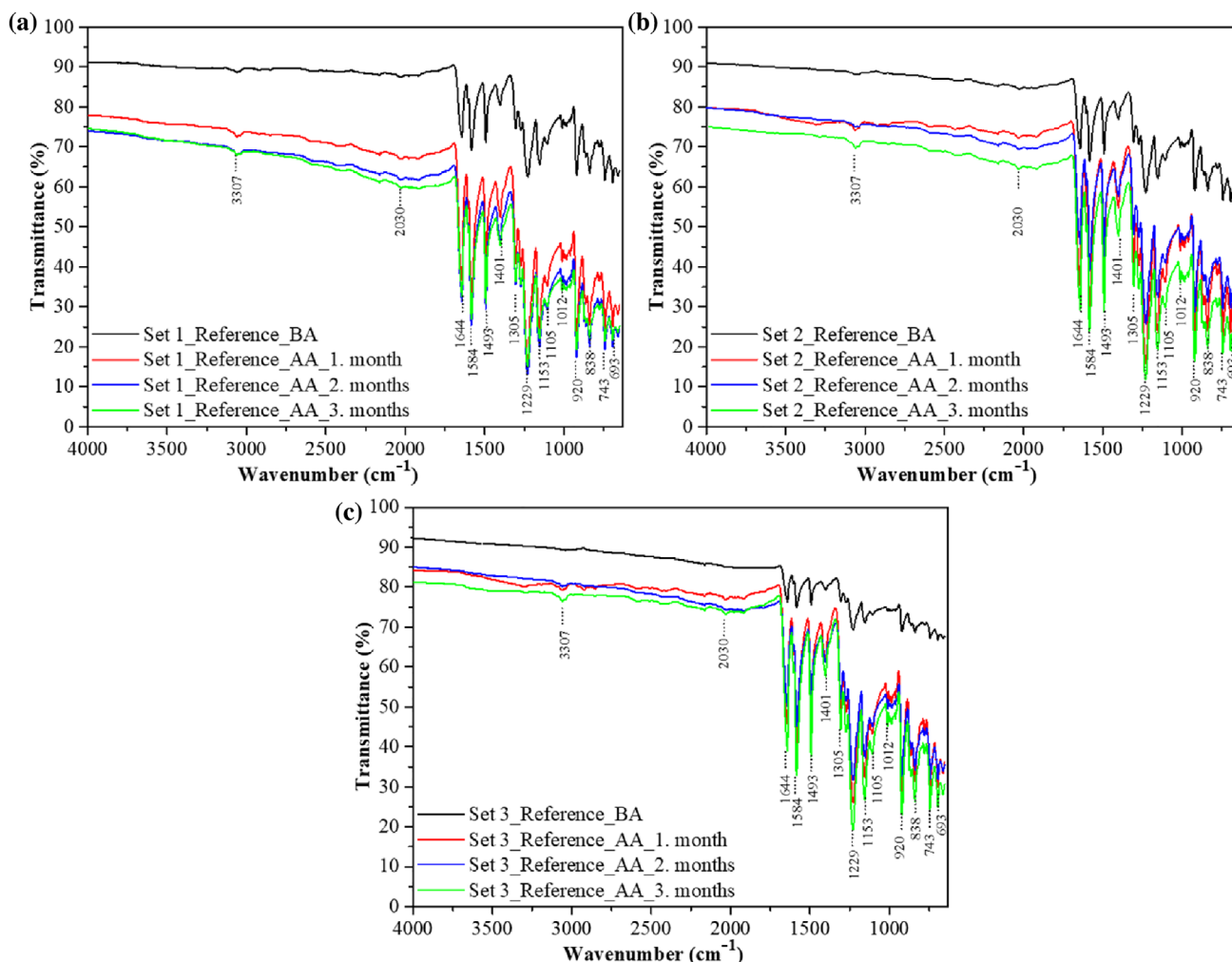
FIGURE 10 FTIR spectra of CF/PEKK samples before and after aging manufactured by process parameters (a) Set 1, (b) Set 2, and (c) Set 3. [Color figure can be viewed at wileyonlinelibrary.com]

3.6 | Dynamic mechanical analysis

DMA thermograms of CF/PEKK composites before and after hydrothermal aging are given in Figure 12 as a function of temperature in terms of storage modulus (E'), loss modulus (E''), and tan delta (δ). E' follows an almost linear trend in the glassy region with a slight positive slope up to the beginning of the viscoelastic region for both BA and AA CF/PEKK samples. The increase in the slope is more significant after the hydrothermal aging period in the reference samples, indicating a moisture concentration gradient in the T_g region through the thickness of the sample and the molecular relaxation times variation depending on the temperature.[51] The CF/PEKK composite has a storage modulus of approximately 20 GPa at room temperature and starts to decrease acutely when the temperature reaches about 147°C. This result is established by the viscoelastic transition associated with the increased mobility of the polymer chains. The E' value

diminishes by almost 25% after the aging period, measured as 15 GPa at room temperature, indicating that the material degrades associated with the plasticization effect due to the aging process.

After the aging process, the viscoelastic region is started at lower temperatures as 130°C with a 10% decrease. This result is evidence that the aging process reduces the service temperature limits of the composite. In addition, the temperature difference for the onset of the viscoelastic transition between the BA and AA samples (17°C) is related to the plasticizing effect of the water and temperature diffused into the matrix leading to the weakening of the interfacial adhesion strength between the fiber and the matrix. The BA and AA composite samples showed similar properties with a continuous decreasing trend up to 250°C in the viscoelastic region.

Loss modulus represents the viscous portion of materials that measures energy dissipation as heat during a deformation cycle. The amount of amorphous structure
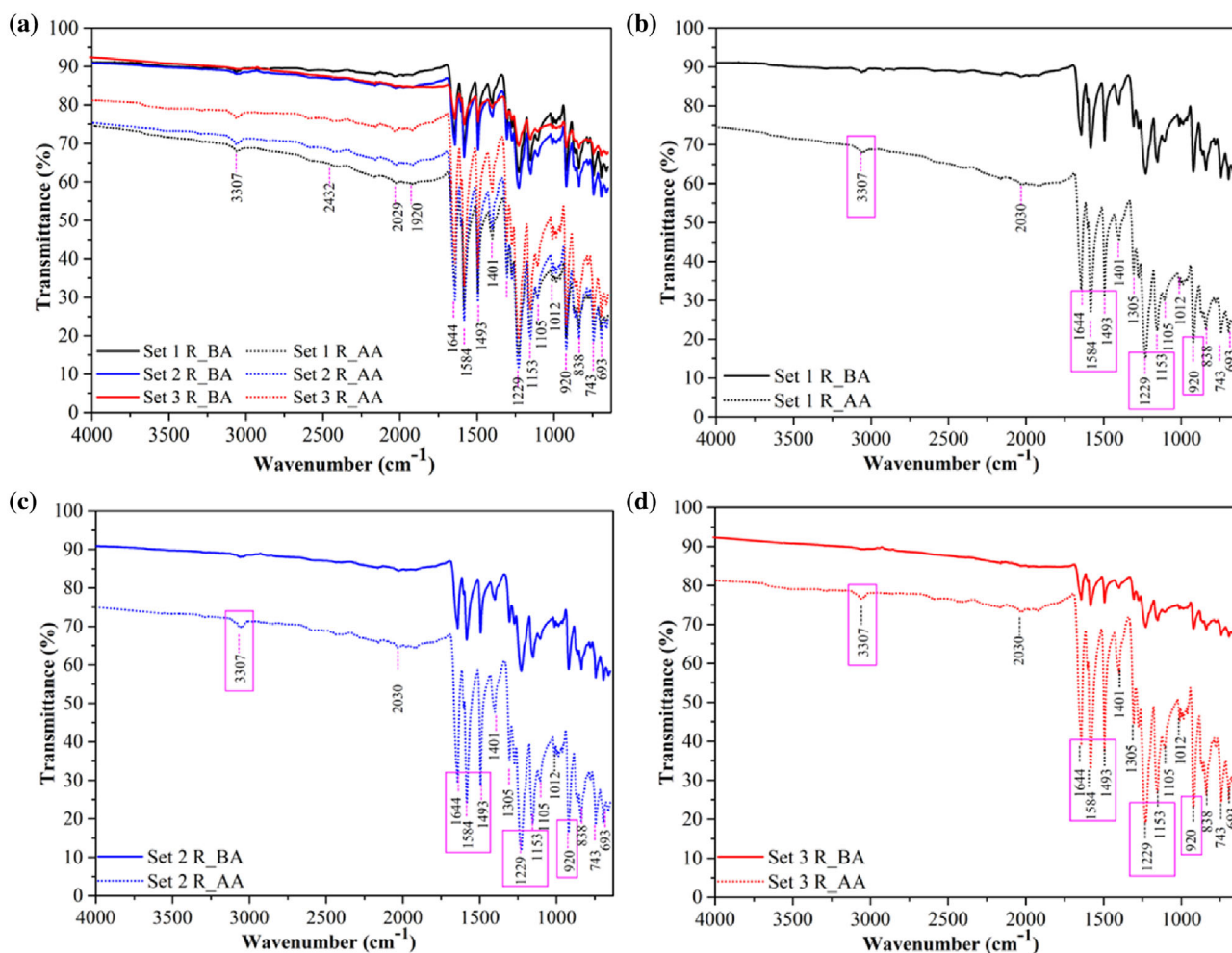
FIGURE 11 FTIR spectra of CF/PEKK samples before and after 90 days of aging (a) all samples, (b) Set 1, (c) Set 2, and (d) Set 3. [Color figure can be viewed at wileyonlinelibrary.com]

in the semicrystalline matrix can be forecasted by comparing the areas below the loss modulus peaks at T_g. The effect of the plasticizing and the interface weakening due to hydrothermal aging is seen in Figure 12b. The intensity in the loss modulus is decreased significantly along with the decreased area under the loss modulus curve after the aging period, which indicates the decrease in the relaxation time of molecular chain motion.[52]

After aging, the loss modulus drops by almost 27%, from 1100 to 800 MPa. A broad secondary peak is observed around 225°C aged samples, which may be related to the restriction of amorphous areas' mobility in the matrix due to postcrystallization. These results are complementary to mechanical test results and evidence that the stiffness of the composite material minimizes after the hydrothermal aging process.[51]

The loss factor or damping is generally accepted as an indicator of the molecular mobility onset and quantifies the degree of viscoelasticity of a sample. As can be seen from Figure 12c, tan (δ) peaks at about 175°C with

a large amplitude before aging, and the amplitude is slightly lower at around 155°C after the aging process. These results are consistent with the DSC results, thus confirming the matrix plasticization of the aging process by water absorption. Moreover, the slight decrease in peak intensities at 225°C AA samples confirm the limitation of chain mobility after crystallization, as seen in Figure 12b.[53]

The DMA thermograms of Reference, Gap, and Overlap CF/PEKK samples manufactured by Set 1 process parameters are given in Figure 13. It is revealed that composite laminates are not affected by gap and overlap defects, considering the initial storage modulus values and the characteristics of the curves (Figure 13a). Even the gap included CF/PEKK sample has a slightly higher initial storage modulus than the reference sample. The onset temperatures of the viscoelastic region remained almost the same before aging (147°C) and after aging (130°C), indicating the hydrothermal aging behavior is not influenced by gap and overlap defects.
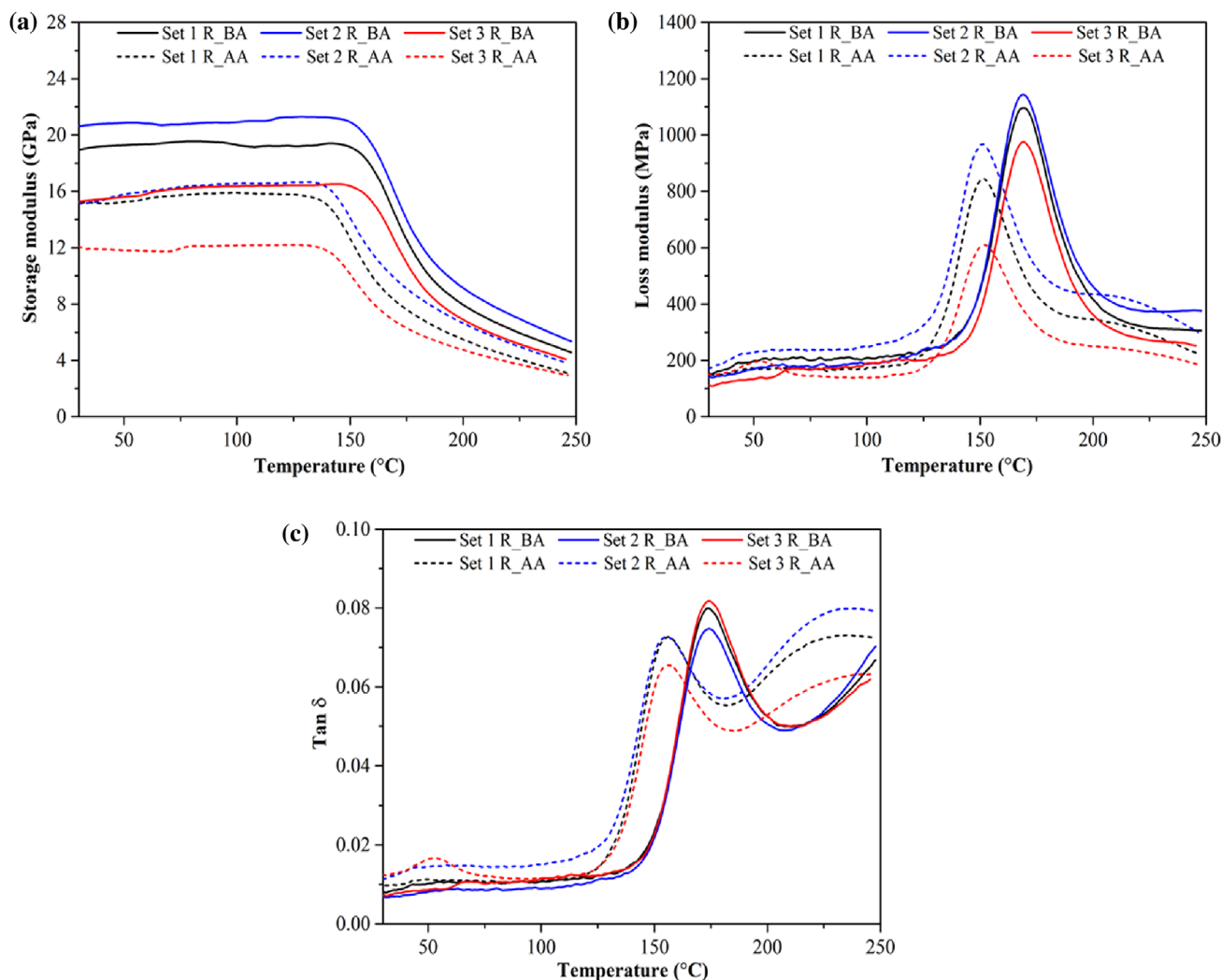
FIGURE 12   DMA thermograms of Reference CF/PEKK samples manufactured with Set 1, Set 2, and Set 3 process parameters before and after aging (a) storage modulus, (b) loss modulus, (c) tan delta (δ). [Color figure can be viewed at wileyonlinelibrary.com]

The loss modulus of gap embedded composite sample manufactured with Set 1 process parameters decreases by almost 25%, from 1100 to 830 MPa, after the aging period, similar to the reference sample. The overlap defect embedded composite sample, on the other hand, shows a slightly lower loss modulus compared with gap defect embedded and reference samples before and after aging. In addition, the postcrystallization curve appears in defect-embedded composite samples but is less pronounced at lower temperatures (220°C). This result is attributed to the relaxation time of the molecular chains' movement. However, there are no outstanding results to associate defects with the aging behavior of composites.

Tan (δ) curves of the composite samples produced using Set 1 process settings are shown in Figure 13c. Since all samples show nearly identical loss factor values compared with the reference sample, it is concluded that gap and overlap defects have little impact on the tan (δ) values. After hydrothermal aging, the loss factors of

defect-embedded samples are identical to those of the reference sample. This finding implies that the thermomechanical characteristics of composites are essentially unaffected by AFP process-induced defects. In essence, there are two essential origins of these outcomes: First, the volume of defects remained low compared with the total volume of the composite since they were generated in only one layer and a bundle, resulting in the unaffected mechanical performance of the composite. Second, the diffusion of water molecules into the voids formed by the defects is limited during aging since the defects remain at the center of the layer.

3.7 | Mechanical characterization results

Flexural stress–strain curves of Reference CF/PEKK samples before and after aging are given in Figure 14. Strain
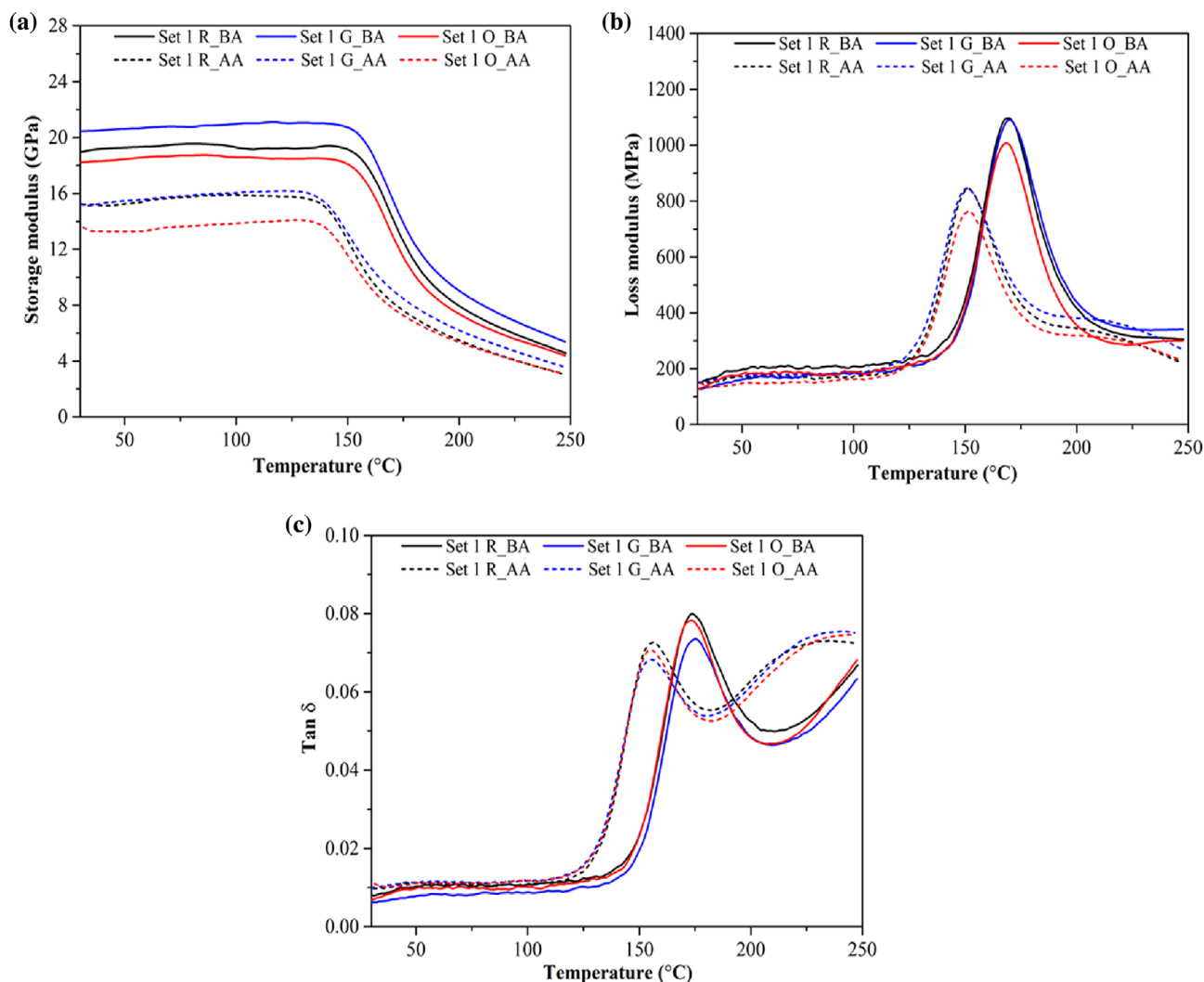
FIGURE 13 DMA thermograms of Reference, Gap, and Overlap CF/PEKK samples manufactured by Set 1 process parameters, before and after aging (a) storage modulus, (b) loss modulus, (c) tan (δ). [Color figure can be viewed at wileyonlinelibrary.com]

values are increased considerably after the hydrothermal aging period due to the matrix plasticization effect. The absorbed water is acted as a plasticizer causing an increase in the ductility.

The flexural stresses of Reference CF/PEKK samples manufactured with Set 1, Set 2, and Set 3 process parameters are 386, 391, and 346 MPa, respectively. However, flexural stresses of the samples manufactured with Set 1, Set 2, and Set 3 process parameters decreased by 19%, 18%, and 27%, respectively. The difference in flexural stresses is more significant in the elastic region (at 0.025 mm/mm).

The highest flexural modulus in reference samples is obtained as 17.58 GPa for Set 2 parameters before aging. Flexural modulus of the composite samples manufactured with Set 1, Set 2, and Set 3 process parameters drop by 16%, 14%, and 17%, respectively. These results are in accordance with DMA analysis, supporting the

plasticization effect of the absorbed water into the matrix. Results obtained from both flexural and DMA analyses of reference composite samples reveal an order of Set 2 > Set 1 > Set 3 in terms of mechanical and thermomechanical properties. The degradation in mechanical properties is related to the triggering of several damage mechanisms due to hydrothermal aging, such as plasticization and swelling caused by expansion forces and stretching of polymer chains.[22]

Matrix plasticization and swelling are directly related to temperature and the amount of water absorbed. The extension of the aging period accelerates the polymer's water absorption and degradation process, especially in the early stages of the aging process. It is seen from the mass gain curve (Figure 6) that the mass gain rise in the first 20 days of the aging period, and then it reaches saturation at the end of the 30th day. The bending tests demonstrate that aging causes
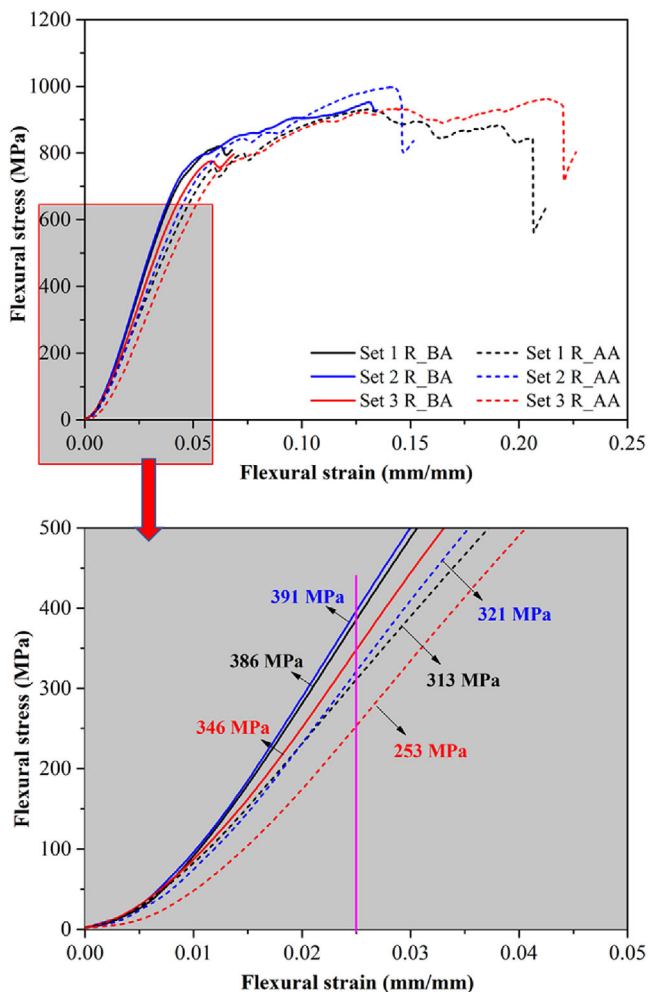
FIGURE 14 Flexural stress–strain curves of Reference CF/PEKK samples manufactured with Set 1, Set 2, and Set 3 process parameters before and after aging. [Color figure can be viewed at wileyonlinelibrary.com]
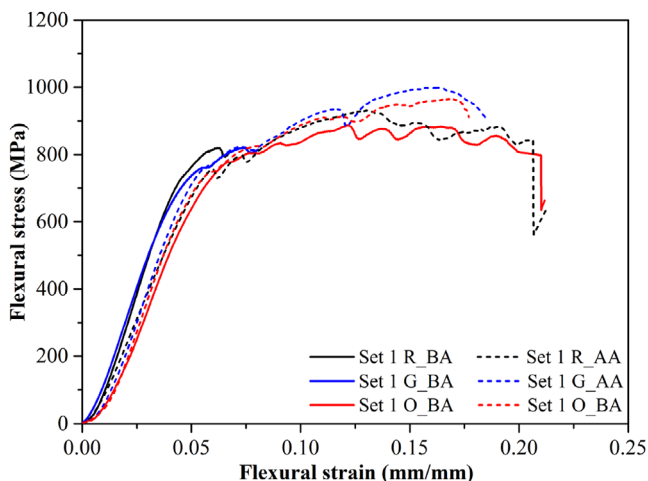

FIGURE 15 Flexural stress–strain curves of Reference, Gap, and Overlap CF/PEKK samples manufactured by Set 1 process parameters before and after aging. [Color figure can be viewed at wileyonlinelibrary.com]
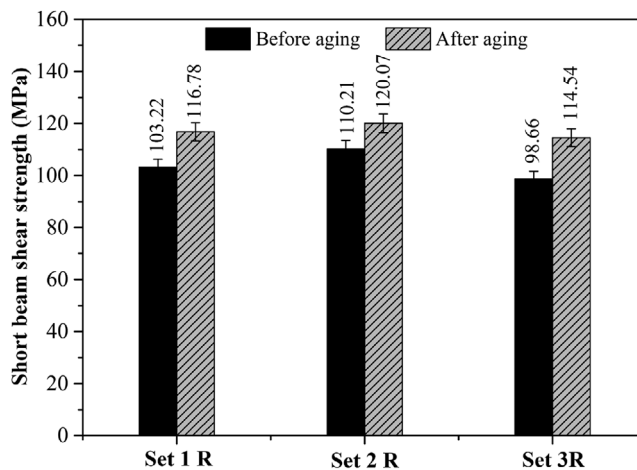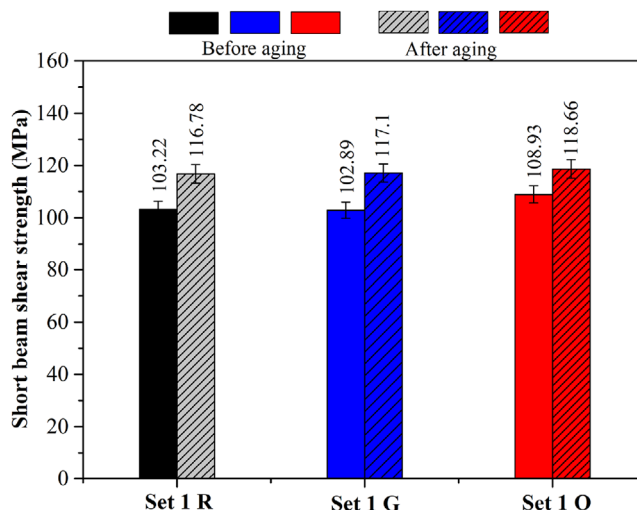

FIGURE 16 Interlaminar shear strength values of Reference CF/PEKK samples manufactured by Set 1, Set 2, and Set 3 process parameters before and after aging.

FIGURE 17 Interlaminar shear strength values of Reference, Gap, and Overlap CF/PEKK samples manufactured by Set 1 process parameters before and after aging. [Color figure can be viewed at wileyonlinelibrary.com]

two main effects: a decrease in flexural stress and an increase in flexural strain values that are consistent with the plasticization of the material.

The flexural stress–strain curves of Reference, Gap, and Overlap CF/PEKK samples are manufactured with the same production parameters (Set 1) before and after aging and are presented in Figure 15. It is noteworthy that the rise in strain values of the samples is due to the plasticization effect of hydrothermal aging. Nevertheless, as in the DMA analysis, the effects of gap and overlap defects on the flexural strength and elastic modulus values are not noticed.

Interlaminar shear stress (ILSS) values of Reference CF/PEKK samples manufactured with different process

Applied Polymer science _WILEY_

FIGURE 18 FESEM images of the fractured surface of the CF/PEKK samples manufactured by Set 1, Set 2, and Set 3 process parameters before and after aging (a) Set 1 R_BA, (b) Set 1 R_AA, (c) Set 2 R_BA, (d) Set 2 R_AA, (e) Set 3 R_BA, and (f) Set 3 R_AA. [Color figure can be viewed at wileyonlinelibrary.com]
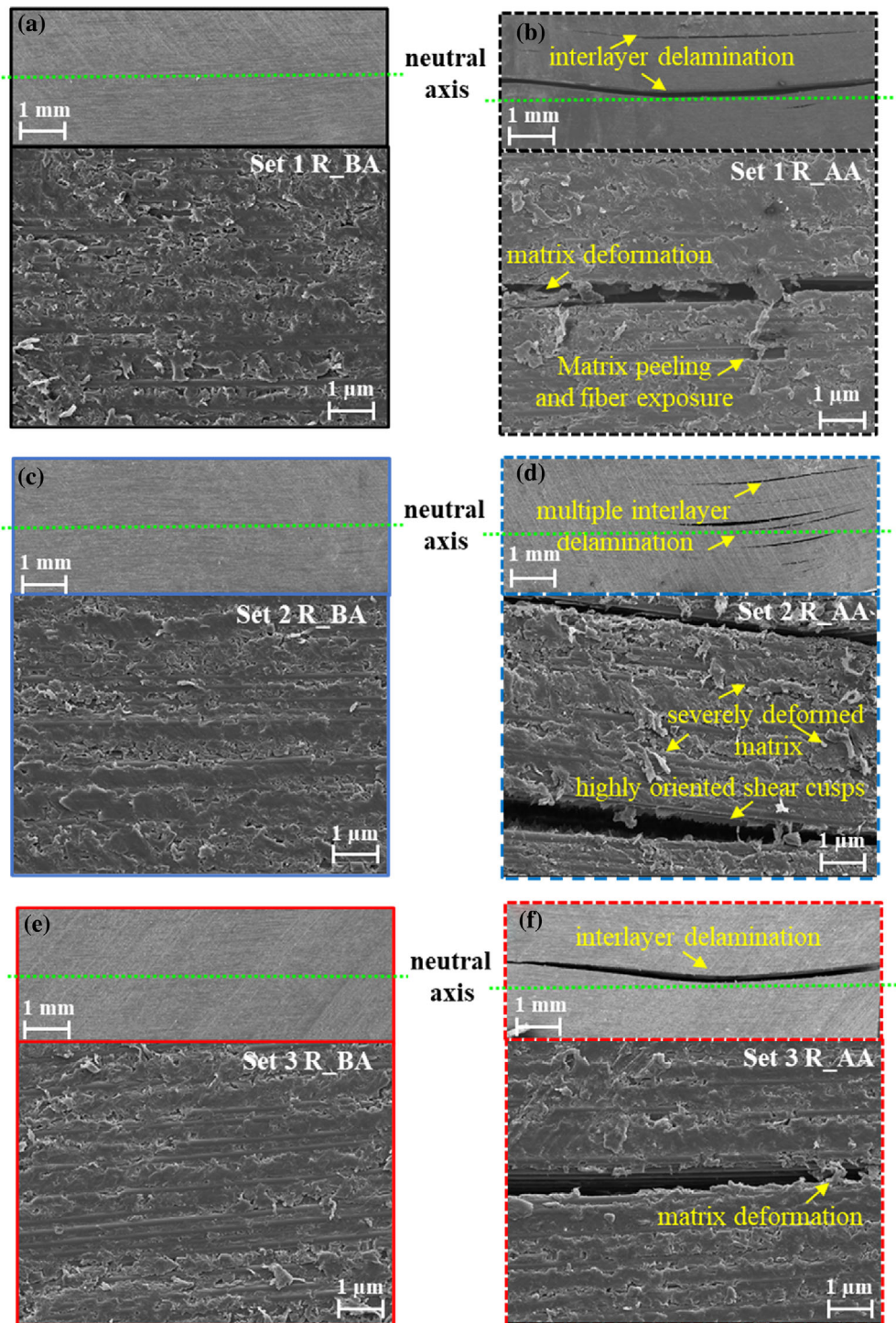
parameters are presented in Figure 16. The shear strength of Reference CF/PEKK samples manufactured with Set 1, Set 2, and Set 3 process parameters are determined to be 103.22, 110.21, and 98.66 MPa, respectively, before aging with increments of 13%, 9%, and 16% after aging, respectively.

Shear strengths of Reference, Gap, and Overlap CF/PEKK samples are almost identical before aging (Figure 17). Similarly, shear strengths enhance by 13%, 14%, and 9% for Reference, Gap, and Overlap CF/PEKK samples,

respectively. This increment in ILSS is attributed to postcuring reactions with the effect of aging.[54] It is thought that high temperature and humidity (water) in composite samples exposed to aging cause a reduction in residual stresses from the curing process of the laminates. The absorbed water likely plasticized the polymer matrix, promoting the removal of residual stresses in the material.[55]

The gap defect is more critical than the overlap defect in terms of the ILSS evaluation. The gap defect can create

local inhomogeneity geometric discontinuities in the composite that affect the mechanical performance. Furthermore, it can accelerate the damage initiation and failure that causes a minimization in the durability of the composite. The decreases and increases in the strength values obtained from the SBS test are explained by the gap defects promoted to create matrix-rich regions and overlap defects promoted to fiber-rich areas in the composite laminate.[27]

After the SBS tests, the damage mechanisms were visualized by SEM analysis, specifically regions close to the neutral axis of samples. Before the hydrothermal conditioning, reference samples produced with different AFP process parameters represent similar damage mechanisms, indicating that the process parameters do not impact the ILSS drastically (Figure 18a,c,e). For hydrothermally conditioned samples, it can be seen that compression and interlaminar shear failures occur when the neutral axis is taken into account. Furthermore, interlayer delamination is observed as the dominant failure mechanism (Figure 18b,d,f). Multiple interlayer delamination is observed intensively in composites produced with Set 2 parameters (Figure 18d) compared with samples produced with Set 1 (Figure 18b), indicating an increased energy absorption under the same loading conditions. Thus, SEM analysis support our previous results that higher mechanical performance can be obtained using Set 2 process parameters.

4 | CONCLUSION

Comprehensive characterization of CF/PEKK composite samples with different process parameters was conducted before and after hydrothermal aging. The study found that reference and gap defect embedded composite samples reached saturation point at 30 days with a 0.2 wt% mass gain, while overlap defect embedded samples reached saturation point with a lower mass gain of 0.15 wt%. The increase in crystallization degrees of CF/PEKK composites after hydrothermal aging was observed in all samples, with the highest increase in Set 1 (14.11%), followed by Set 3 (10.29%) and Set 2 (8.70%). DMA analysis showed a decrease in thermo-mechanical properties of all samples after aging, but gap and overlap defects had minimal effect on the properties. The increase in flexural strain values and decrease in flexural properties were attributed to various damage mechanisms triggered by hydrothermal aging, such as plasticization/swelling caused by expansion forces and stretching of polymeric chains. However, ILSS values were increased due to plasticizing the polymer matrix and reducing residual stresses.

The process parameters order in terms of providing better mechanical and thermo-mechanical performance

appointed as Set 2 (600 N, 0.1 m/s) > Set 1 (300 N, 0.1 m/s) > Set 3 (600 N, 0.4 m/s) as regards the comprehensive tests and analyzes results. The optimum process parameters of AFP are determined as Set 2 (600 N, 0.1 m/s). In case of a possible gap and overlap defect during laying-up, the effect of the defect will be minimized if the consolidation force and the lay-up speed are set to 600 N and 0.1 m/s, respectively, on the next layer.

DATA AVAILABILITY STATEMENT
The raw data required to reproduce these findings are available from the corresponding author upon request.

ORCID
Emine Feyza Sukur https://orcid.org/0000-0003-2644-880X
Volkan Eskizeybek https://orcid.org/0000-0002-5373-0379
Hatice S. Sas https://orcid.org/0000-0002-5179-2509
Mehmet Yildiz https://orcid.org/0000-0003-1626-5858

REFERENCES
[1] I. Schiel, L. Raps, A. R. Chadwick, I. Schmidt, M. Simone, S. Nowotny, *Adv. Manuf. Polym. Compos. Sci.* **2020**, *6*, 191.

[2] K. Yassin, M. Hojjati, *J. Thermoplast. Compos. Mater.* **2018**, *31*, 1676.

[3] J. H. Shin, D. Kim, T. Centea, S. R. Nutt, *Compos. Part A: Appl. Sci. Manuf.* **2019**, *119*, 154.

[4] E. F. Sukur, S. Elmas, M. Seyyednourani, V. Eskizeybek, M. Yildiz, H. S. Sas, *J. Appl. Polym. Sci.* **2022**, *139*, 139.

[5] E. F. Sukur, *Polym. Compos.* **2023**, *44*, 2530. https://doi.org/10.1002/pc.27261

[6] Y. Cheng, F. Sun, Y. Zhang, F. Tao, *J. Ind. Inf. Integr.* **2019**, *15*, 207.

[7] C. Wanigasekara, E. Oromiehie, A. Swain, B. G. Prusty, S. K. Nguang, *J. Ind. Inf. Integr.* **2021**, *22*, 100197.

[8] O. Baho, G. Ausias, Y. Grohens, J. Férec, *Int. J. Adv. Manuf. Technol.* **2020**, *110*, 2105.

[9] Q. Song, W. Liu, J. Chen, D. Zhao, C. Yi, R. Liu, Y. Geng, Y. Yang, Y. Zheng, Y. Yuan, *Polymers (Basel)* **2022**, *14*, 1401.

[10] C. M. Stokes-Griffin, P. Compston, *Compos. Part A: Appl. Sci. Manuf.* **2015**, *78*, 274.

[11] Z. Qureshi, T. Swait, R. Scaife, H. M. El-Dessouky, *Compos. Part B: Eng.* **2014**, *66*, 255.

[12] R. Harik, C. Saidy, S. J. Williams, Z. Gurdal, B. Grimsley, *Int. SAMPE Tech. Conf.* **2018**, 2018.

[13] K. Fayazbakhsh, M. Arian Nik, D. Pasini, L. Lessard, *Compos. Struct.* **2013**, *97*, 245.

[14] X. Li, S. R. Hallett, M. R. Wisnom, *Sci. Eng. Compos. Mater.* **2015**, *22*, 115.

[15] W. E. Guin, J. R. Jackson, C. M. Bosley, *Compos. Part A: Appl. Sci. Manuf.* **2018**, *115*, 66.

[16] W. Woigk, S. R. Hallett, M. I. Jones, M. Kuhtz, A. Hornig, M. Gude, *Compos. Struct.* **2018**, *201*, 1004.

[17] T. Zenker, F. Bruckner, K. Drechsler, *Adv. Manuf. Polym. Compos. Sci.* **2019**, *5*, 184.

[18] M. H. Nguyen, P. Davidson, A. M. Waas, *Int. J. Mater. Form.* **2021**, *14*, 105.

[19] N. Guermazi, A. Ben Tarjem, I. Ksouri, H. F. Ayedi, *Compos. Part B: Eng.* **2016**, *85*, 294.

[20] K. Shetty, R. Bojja, S. Srihari, *Adv., Compos. Lett.* **2020**, *29*, 2633366X2092652.

[21] E. F. Sukur, S. Elmas, M. Seyyednourani, V. Eskizeybek, M. Yildiz, H. S. Sas, *Polym. Compos.* **2022**, *43*, 8396.

[22] N. Z. Borba, J. F. dos Santos, S. T. Amancio-Filho, *Compos. Struct.* **2021**, *255*, 112871.

[23] T. S. Plagianakos, K. Muñoz, D. Saenz-Castillo, M. M. Mendias, M. Jiménez, V. Prentzias, *Aerospace* **2020**, *7*, 1.

[24] R. L. Mazur, G. M. Cândido, M. C. Rezende, E. C. Botelho, *J. Thermoplast. Compos. Mater.* **2016**, *29*, 1429.

[25] S. Sun, Z. Han, J. Zhang, H. Jin, Y. Wang, *Compos. Struct.* **2021**, *259*, 113215.

[26] R. Wehbe, C. Sacco, A. Baz Radwan, M. Albazzan, R. Harik, *Compos. Part C: Open Access* **2020**, *2*, 100036.

[27] M. Lan, D. Cartié, P. Davies, C. Baley, *Compos. Part A: Appl. Sci. Manuf.* **2016**, *82*, 198.

[28] O. Baho, G. Ausias, Y. Grohens, J. Férec, *Int. J. Adv. Manuf. Technol.* **2020**, *1107*, 2020.

[29] M. Perner, S. Algermissen, R. Keimer, H. P. Monner, *Robot. Comput. Integr. Manuf.* **2016**, *38*, 82.

[30] A. C. Bottene, W. L. Nunes de Mello, R. Z. Hemerly de Almeida, *Int. J. Veh. Struct. Syst.* **2012**, *4*, 4.

[31] J. J. Gangloff, T. A. Cender, V. Eskizeybek, P. Simacek, S. G. Advani, *J. Compos. Mater.* **2017**, *51*, 2757.

[32] L. Quiroga Cortés, N. Caussé, E. Dantras, A. Lonjon, C. Lacabanne, *J. Appl. Polym. Sci.* **2016**, *133*, 43396.

[33] A. Barzegar, S. Karimi, E. F. Sukur, H. S. Sas, M. Yildiz, *J. Reinf. Plast. Compos.* **2022**, 073168442211434, Epub ahead of print. https://doi.org/10.1177/07316844221143448

[34] S. Karimi, P. Y. Louyeh, A. Barzegar, M. Yildiz, H. S. Sas, *J. Reinf. Plast. Compos.* **2023**, 07316844231166078, Epub ahead of print. https://doi.org/10.1177/07316844231166078

[35] D. Saenz-Castillo, M. I. Martín, S. Calvo, F. Rodriguez-Lence, A. Güemes, *Compos. Part A: Appl. Sci. Manuf.* **2019**, *121*, 308.

[36] M. B. Gruber, I. Z. Lockwood, T. L. Dolan, S. B. Funck, J. J. Tierney, P. Simacek, J. W. Gillespie, S. G. Advani, B. J. Jensen, R. J. Cano, B. W. Grimsley. Proc. 2012. SAMPE Conf. Exhib. 2012.

[37] A. Bergeret, I. Pires, M. P. Foulc, B. Abadie, L. Ferry, A. Crespy, *Polym. Test.* **2001**, *20*, 753.

[38] C. S. P. Borges, A. Akhavan-Safar, E. A. S. Marques, R. J. C. Carbas, C. Ueffing, P. Weißgraeber, L. F. M. da Silva, *Materials (Basel)* **2021**, *14*, 1.

[39] M. Eftekhari, A. Fatemi, *Polym. Test.* **2016**, *51*, 151.

[40] X. Wang, Z. Hou, Y. Yang, *Fibers Polym.* **2022**, *23*, 502.

[41] K. Iggui, M. Kaci, N. Le Moigne, A. Bergeret, *Polym. Compos.* **1878**, **2021**, 42.

[42] M. Coulson, L. Q. Cortés, E. Dantras, A. Lonjon, C. Lacabanne, *J. Appl. Polym. Sci.* **2018**, *135*, 46456.

[43] L. O. Dandy, G. Oliveux, J. Wood, M. J. Jenkins, G. A. Leeke, *Polym. Degrad. Stab.* **2015**, *112*, 52.

[44] A. M. Al-Khafaji, T. I. Hamad, *Int. Med. J.* **2021**, *28*, 29.

[45] X. Hu, S. Mei, F. Wang, J. Qian, D. Xie, J. Zhao, L. Yang, Z. Wu, J. Wei, *Bioact. Mater.* **2021**, *6*, 928.

[46] B. Yuan, Q. Cheng, R. Zhao, X. Zhu, X. Yang, X. Yang, K. Zhang, Y. Song, X. Zhang, *Biomaterials* **2018**, *170*, 116.

[47] F. Xiao, Y. Zhai, Y. Zhou, X. Xu, Y. Liu, X. Ma, X. Gu, W. Wang, *Surf. Coatings Technol.* **2021**, *416*, 127158.

[48] S. Fan, C. Gao, G. Yang, Y. Zhang, C. Zhang, N. Song, S. Zhang, P. Zhang, Z. Zhang, S. Ke, *Tribol. Int.* **2021**, *153*, 106601.

[49] B. Ghosh, F. Xu, X. Hou, *J. Mater. Sci.* **2021**, *56*, 10326.

[50] A. A. Mohammed, E. S. Al-Hassani, J. K. Oleiwi, S. R. Ghaffarian, *Mater. Res. Express* **2019**, *6*, 125405.

[51] R. L. Mazur, P. C. Oliveira, M. C. Rezende, E. C. Botelho, *J. Reinf. Plast. Compos.* **2014**, *33*, 749.

[52] T. L. Nguyen, F. Bédoui, P.-E. Mazeran, M. Guigon, *Polym. Eng. Sci.* **2015**, *55*, 397.

[53] A. Saleem, L. Frormann, A. Iqbal, *Polym. Compos.* **2007**, *28*, 785.

[54] S. Marouani, L. Curtil, P. Hamelin, *Compos. Part B: Eng.* **2020**, *2012*, 43.

[55] A. P. Cysne Barbosa, A. P. P. Fulco, E. S. S. Guerra, F. K. Arakaki, M. Tosatto, M. C. B. Costa, J. D. D. Melo, *Compos. Part B: Eng.* **2017**, *110*, 298.